

Automotive Object Detection via Learning Sparse Events by Spiking Neurons

Hu Zhang, Yanchen Li, Liziwei Leng, Kaiwei Che, Qian Liu, Qinghai Guo, Jianxing Liao, and Ran Cheng

Abstract—Event-based sensors, distinguished by their high temporal resolution of $1\mu\text{s}$ and a dynamic range of 120 dB , stand out as ideal tools for deployment in fast-paced settings like vehicles and drones. Traditional object detection techniques that utilize Artificial Neural Networks (ANNs) face challenges due to the sparse and asynchronous nature of the events these sensors capture. In contrast, Spiking Neural Networks (SNNs) offer a promising alternative, providing a temporal representation that is inherently aligned with event-based data. This paper explores the unique membrane potential dynamics of SNNs and their ability to modulate sparse events. We introduce an innovative spike-triggered adaptive threshold mechanism designed for stable training. Building on these insights, we present a specialized spiking feature pyramid network (SpikeFPN) optimized for automotive event-based object detection. Comprehensive evaluations demonstrate that SpikeFPN surpasses both traditional SNNs and advanced ANNs enhanced with attention mechanisms. Evidently, SpikeFPN achieves a mean Average Precision (mAP) of 0.477 on the GEN1 Automotive Detection (GAD) benchmark dataset, marking a significant increase of 9.7% over the previous best SNN. Moreover, the efficient design of SpikeFPN ensures robust performance while optimizing computational resources, attributed to its innate sparse computation capabilities.

Index Terms—Autonomous driving, object detection, deep learning, spiking neural networks.

I. INTRODUCTION

OBJECT detection is fundamental in computer vision, with applications ranging from face recognition to vehicle tracking and the identification of smaller objects [1], [2]. Traditionally, such tasks rely on frame-based cameras. However, these often produce images that are blurred or poorly exposed, especially in high-speed or challenging lighting conditions, common in scenarios like emergency vehicle detection. Addressing this gap, the recently advanced Dynamical Vision Sensor (DVS), a.k.a. the event-based sensor [3]–[8], offers a compelling alternative. Unlike traditional sensors, the DVS draws inspiration from retinal functionalities and is adept at registering pixel intensity variations. With its remarkable temporal resolution of $1\mu\text{s}$ and a dynamic range of 120 dB , it is able to effectively record asynchronous events instigated by shifts in pixel brightness.

Despite the appealing characteristics, the unique nature of DVS also brings challenges. Its event-driven data is sparse

Hu Zhang, Yanchen Li, and Ran Cheng are with the Department of Computer Science and Engineering, Southern University of Science and Technology, Shenzhen 518055, China. Kaiwei Che is with the Department of Electrical and Electronic Engineering, Southern University of Science and Technology, Shenzhen 518055, China. (e-mail: ranchengcn@gmail.com)

Liziwei Leng, Qian Liu, Qinghai Guo and Jianxing Liao are with the Advanced Computing and Storage Lab, Huawei Technologies Co., Ltd., Shenzhen 518055, China. (e-mail: lengliziwei@huawei.com) (Corresponding authors: Liziwei Leng and Ran Cheng.)

and unpredictable, making traditional object detection methods based on Artificial Neural Networks (ANNs) less effective. While there have been efforts to preprocess such events using various architectures and algorithms [9], [10], they often come with substantial computational and latency costs. By contrast, the Spiking Neural Networks (SNNs) [11], [12] introduce a new paradigm, resembling the brain's functioning by transmitting information through discrete spikes. Their inherent efficiency, marked by sparse activations and multiplication-free inferences, makes them ideal for managing the dynamic, sparse data from event-driven sensors.

Recent breakthroughs in surrogate gradient (SG) algorithms [13], [14] have paved the way for efficient training of deep SNNs in image classification domains [15]–[19]. However, when it comes to more intricate vision tasks like automotive object detection [20]–[22], SNNs still find themselves trailing behind the established prowess of ANNs. Though significant strides have been made in enhancing ANNs for challenging object detection tasks [23]–[27], directly transposing these refined ANN architectures onto the SNN framework often leads to compromised performance and heightened latency. Such performance deficits are glaring in tasks that necessitate sophisticated neural network adjustments [20], [28], [29]. Moreover, while current efforts focus on converting ANNs to SNNs [30]–[34], these approaches grapple with inherent challenges. These primarily arise when integrating the dynamic nature of SNNs with the foundational attributes of ANNs, which frequently results in the underutilization of the unique temporal and sparse characteristics inherent to SNNs — essential for handling event-driven data efficiently. The inherent differences in data representation and processing between the two neural architectures often result in deviations, undermining both the accuracy and computational performance of the neural system.

In response to these challenges, we delve deeper into the temporal dynamics inherent to spiking neurons, aiming to develop an approach characterized by minimal computational requirements and efficient response times, especially crucial for swiftly varying events. Leveraging our findings, we design a tailored spiking feature pyramid network (SpikeFPN) for event-based automotive object detection, which harmoniously blends the unique neuronal properties with surrogate gradient training to achieve optimal performance. Our primary contributions are delineated as follows:

- 1) We have delved into the inherent temporal dynamics of spiking neurons, particularly focusing on membrane potential dynamics and adaptive thresholds. Our comprehensive study not only reveals their intrinsic strengths in managing rapid event modulations but also underscores

their pivotal role in amplifying the robustness of features derived from sparse events. The insights gained ensure stable and efficient training phases, optimizing the network's performance in real-world scenarios.

- 2) We have designed an event-driven SpikeFPN tailored specifically for automotive object detection, leveraging the self-adaptive mechanism inspired by neocortex neuron adaptation. This design foundation captures the unique temporal dynamics of spiking neurons, presenting a novel approach to object detection in automotive scenarios. Moreover, building upon the core principles of our SpikeFPN, we have adopted a surrogate gradient training to optimize the encoder's structure.
- 3) Our proposed SpikeFPN has demonstrated promising performance, surpassing previous SNN models and advanced ANNs with attention mechanisms. It attains a noteworthy mean Average Precision (mAP) of 0.477 on the GEN1 Automotive Detection (GAD) benchmark dataset, marking a substantial advancement by outperforming the previous best SNN by 9.7%. Additionally, our design is a testament to efficiency—combining a streamlined architecture with impressive accuracy, all while significantly reducing computation costs.

The structure of this paper is outlined as follows: Section II provides the foundational background relevant to our study; Section III delves into the intricacies of the proposed SpikeFPN, detailing its architectural components and elaborating on the neural behavior and adaptive strategies employed; Section IV showcases our experimental approaches, the methodologies adopted, and the corresponding results, affirming the effectiveness of our design; finally, the paper culminates with conclusions drawn in Section V.

II. BACKGROUND

A. Event-based Object Detection

Event cameras, possessing outstanding temporal resolution and dynamic range, are optimally suited for scenarios demanding rapid object tracking, variable lighting conditions, and minimal latency. Nonetheless, the intrinsic dynamism of event camera data clashes with conventional deep learning paradigms grounded in frame-based methodologies. Typically, to counter this incongruence, events undergo preprocessing to transform into denser representations before network processing. Various methodologies, both handcrafted and automated, have been championed for this transformation, encompassing event frames [35]–[40], time or event-number stacking [41], voxel grids [42], the event queue approach [43], LSTM grids [44], and discrete time convolutions [45]. For sparse event data, asynchronous convolutions have also been broached [46], [47], with the latter notably applied to the GEN1 Automotive Detection (GAD) dataset acquired with the GEN1 sensor for event-driven automotive object detection tasks [48]. The work by [9] accentuated a convolutional LSTM network coupled with a temporal consistency loss, amplifying training outcomes. ASTMNet [10] showcased an innovative adaptive sampling protocol, fusing temporal attention and memory modules, and clocked unparalleled accuracy levels.

B. Deep SNNs for Vision Tasks

Neuromorphic hardware evolution has invigorated the enthusiasm for harnessing SNNs in challenging vision-based deep learning tasks [49]–[56]. When amalgamated with event cameras, these neuromorphic ecosystems promise unprecedented power efficiency coupled with minimal latency [57]. Training deep SNNs revolves predominantly around two pivotal methodologies: the conversion from ANNs to SNNs and direct training.

The conversion strategy revolves around approximating real-valued activations with spiking dynamics [33], [58]. While this strategy manifests high accuracy levels, it is weighed down by heightened latency owing to spike rate accumulations, rendering it less effective for rapid event processing. [29] introduced a spiking version of YOLO for object detection and achieved a virtually identical performance on the PASCAL VOC [59] and MS COCO datasets [60], albeit demanding thousands of timesteps for convergence. Recent endeavors have managed to curb the latency post conversion [30], [31], yet the scalability of these methodologies to more intricate architectures beyond mere image classification remains nebulous.

Direct training, on the other hand, leverages surrogate gradient (SG) functions to mimic backpropagation gradients [13], [14], [61]. Owing to advancements like tailored normalization, SG, and loss function crafting [15], [18], [19], [62], directly trained SNNs have been attaining competitive accuracies on strenuous benchmark tasks like ImageNet, demanding minimal simulation steps for convergence. These milestones have catalyzed their expansion into other event-centric vision tasks, from optical flow assessment [28] to video reproduction [63] and object recognition [20]. Yet, many of these endeavors remain encumbered by rather simplistic handcrafted architectures and often don't match the accuracy prowess of elite ANNs. Recent breakthroughs, for instance, those by [64]–[66], underscore that spike-centric differentiable hierarchical searches can considerably elevate SNN performance across a spectrum of event-driven vision tasks, including arduous ones like deep stereo and semantic segmentation.

C. Feature Pyramid Networks

Feature Pyramid Networks (FPNs) are central components of numerous object detection systems, with their capacity to exploit multi-scale feature information enhancing overall system performance [67]–[69]. The original FPN design was introduced by [70], which built on traditional pyramid methods by efficiently leveraging single-scale image input, forming a foundation for subsequent advancements in the field.

Among these advancements, the FaPN by [71] incorporated a feature alignment module, achieving a state-of-the-art refinement over the conventional FPN design. In contrast to the fusion-based approach, the SSD method, proposed by [72], delegated different stages of feature maps to detect objects of distinct scales. Several integrated techniques, such as those found in [73]–[77], fused features from diverse stages, predominantly using a top-down unidirectional fusion method—a prevailing FPN fusion mode in modern object detection models.

The PANet [78] made strides by pioneering the concept of bottom-up secondary bi-directional fusion, shedding light on the potential benefits of bi-directional fusion. Further expanding on the capabilities of FPNs, the ASFF [79] incorporated an attention mechanism, while complex bidirectional fusion techniques, such as those in [80], [81], ventured into more intricate fusion dynamics. A novel approach was taken by the Recursive-FPN [82], wherein the fused output of the FPN was reintegrated into the backbone, initiating an additional loop and marking a new state-of-the-art. Further bridging the gap between conventional neural networks and the emerging field of SNNs, recent work [83] endeavored to combine feature pyramid structures with SNNs.

III. METHOD

This section begins with the representation of event data. Subsequently, it introduces the proposed feature-pyramid-centric spiking neural network underpinned by a self-adaptive spiking neuron model. This model effectively leverages temporal dynamics, ensuring compatibility with the highly variable event information flow. To clarify the network's design, the foundational architecture is elucidated, highlighting modules such as the primary backbone. The section further presents the formulation of the adaptive spiking neural propagation model intrinsic to the network. Ultimately, the strategy for employing approximate information to address the non-differentiability challenge during training is elaborated upon.

A. Event Data Representation

Traditional cameras capture visual information in the form of images. In contrast, a DVS detects individual pixel changes in their receptive fields, registering changes in luminance and labeling these as “events”. Typically, an event is recorded in a tuple format (t, x, y, p) , where t represents the timestamp of the event occurrence; x, y denote the two-dimensional pixel coordinates where the event is registered; and p indicates the polarity of the event, reflecting the direction of luminance change.

In order to effectively encode the inherently discrete event data while retaining its temporal nuances, we employ the Stacking Based on Time (SBT) method for event preprocessing as presented by Wang *et al.* [41]. The SBT approach, recognized for its real-time processing and low computational overhead, has been integrated into the accumulator modules of mainstream event sensors. Beyond mere data compression, the SBT preserves the granular temporal information of the event stream. It amalgamates events into temporally contiguous frames, facilitating the downstream Spiking Neural Network (SNN) to learn from this rich temporal dataset. Within a single stack input into the detection model, the SBT method partitions the event data uniformly based on the time interval Δt . It then compresses this data to yield a set of frames. Assuming the event data in the stack can be subdivided into n equal time intervals, the value of each pixel in the i -th frame is characterized by the aggregated polarity of events as:

$$P(x, y) = \text{sign} \left(\sum_{t \in T} p(x, y, t) \right), \quad (1)$$

where P designates the pixel value at coordinates (x, y) ; t represents the timestamp; p denotes the event's polarity; and $T \in [(i-1)\Delta t/n, i\Delta t/n]$ specifies the timeframe of events consolidated into a single frame.

While the SBT approach offers substantial utility, alternative event data representation techniques exist, some of which closely resemble our encoding method. Although not integrated into our model, these techniques occasionally offer superior performance in specific contexts. For instance, in scenarios characterized by infrequent events during the consolidation interval, the SBT might yield a frame with notably sparse values. In such cases, the Stacking Based on the number of Events (SBE) method, as introduced by Wang *et al.* [41], emerges as a more apt choice. The SBE methodology builds a frame using a predetermined number of events, providing an effective solution to the challenge of sparse event representation. To comprehensively evaluate the influence of various event encoding strategies on object detection tasks, we have compared multiple encoding modalities in the ablation studies detailed in Section IV-B3.

B. Network Design

In response to the unique challenges of event-based object detection, we design a feature-pyramid-centric spiking neural network built upon a threshold-adaptive spiking unit mechanism. The foundational neuron unit, characterized by self-adaptive and spiking attributes, seamlessly adapts to intricate scenarios. Coupled with the network's feature pyramid module, it provides a robust architecture. A multi-head prediction mechanism layered on top further enhances detection accuracy. This section delves into a detailed discussion of the network's overall structure, encapsulating the design intricacies of both the backbone and the feature pyramid module. Subsequently, we illustrate the behavior and propagation mechanisms of the spiking neuron unit incorporated within our approach.

1) *Network Architecture*: The network adopts a feature pyramid architecture which emanates from a downsampling paradigm, employing foundational cell units to sculpt the encoding backbone. Spiking feature maps, derived from the concluding three stages of the backbone, amalgamate to create the spiking feature pyramid—a focal element of the overarching network design as depicted in Fig. 1. This component plays a pivotal role in feature extraction. A comprehensive visualization of the backbone's output feature map, in conjunction with the entire network, can be found in Table I. The inaugural two spiking stem layers of our architecture facilitate a twofold downsampling of the feature map. This is succeeded by 10 spiking cells, which together forge a four-stage downsampling lattice. Outputs from the terminal cells across stages 2, 3, and 4 are relayed to the feature pyramid. The aggregate network achieves a peak downsampling ratio of 32. In the following, we further elucidate the intricate design elements of the backbone, complemented by the subsequent spiking feature pyramid network.

As depicted in Fig. 2, the encoder backbone adopts a multi-stage downsampling strategy. This architecture consists of an initial two spiking stem layers, followed by a sequence of ten

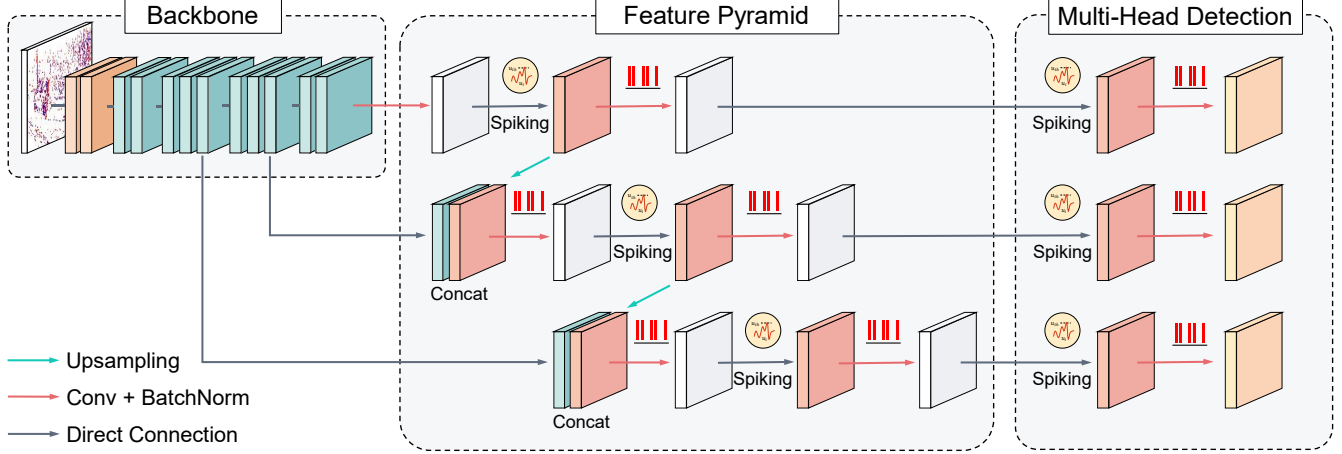


Fig. 1. Overview of the proposed spiking feature pyramid network. The design encompasses an encoder backbone facilitated by a multi-stage spiking network. Different stages of the backbone contribute to the integrated spiking feature pyramid. Subsequent to this, a multi-head prediction module processes the feature pyramid's output through parallel spiking convolution layers, culminating in the generation of multiple prediction boxes. These are ultimately refined using the Non-Maximum Suppression (NMS) method. Notably, the entire network operates on spike-based computation, offering the advantage of multiplication-free inference.

TABLE I
DETAILED ARCHITECTURE SETTINGS OF THE PROPOSED SPIKING FEATURE PYRAMID NETWORK. THE ILLUSTRATION ENCOMPASSES THE ENCODER BACKBONE, THE FEATURE PYRAMID, AND THE MULTI-HEAD PREDICTION MODULE. HERE, C REPRESENTS THE NUMBER OF CLASSES, WHILE K SIGNIFIES THE NUMBER OF ANCHORS.

Module	Layer	Output Feature Map $c \times h \times w$
Backbone	Stem 0	$48 \times 128 \times 128$
	Stem 1	$96 \times 64 \times 64$
	Cell 0	$96 \times 64 \times 64$
	Cell 1	$96 \times 64 \times 64$
	Cell 2	$192 \times 32 \times 32$
	Cell 3	$192 \times 32 \times 32$
	Cell 4	$192 \times 32 \times 32$
	Cell 5	$384 \times 16 \times 16$
	Cell 6	$384 \times 16 \times 16$
	Cell 7	$384 \times 16 \times 16$
Feature Pyramid	Cell 4 \rightarrow p1	$96 \times 32 \times 32$
	Cell 7 \rightarrow p2	$192 \times 16 \times 16$
	Cell 9 \rightarrow p3	$384 \times 8 \times 8$
Multi-Head Prediction	p1 \rightarrow d1	$K \times (C + 5) \times 32 \times 32$
	p2 \rightarrow d2	$K \times (C + 5) \times 16 \times 16$
	p3 \rightarrow d3	$K \times (C + 5) \times 8 \times 8$

spiking cells. Through the downsampling process, the spatial resolution of the feature map is reduced by half, while the channel size experiences a twofold increase. Each spiking stem layer comprises a convolutional layer, batch normalization (which can be integrated into convolution weights during test inference, as suggested by [84]), and a spiking activation function. These layers are meticulously crafted to spearhead initial feature extraction and channel modulation. Each spiking cell is structured around three spiking nodes, with this arrangement being reiterated across multiple layers. The initial pair of nodes procure inputs from the preceding two cells, while the third node assimilates input from its immediate two predecessors. The feature maps across all nodes maintain a consistent size. Their respective outputs

converge, forming the collective output of the cell. Within each node, operations stemming from various edges aggregate at the membrane potential level before undergoing the spiking activation function. The interconnections within the spiking cell are heuristically determined to harmonize inference speed with accuracy.

Post the processing through the backbone, fundamental features are discerned. However, subsequent operations are requisite to achieve the anticipated results. The lower spatial resolution features from the pyramid undergo upsampling via the nearest interpolation method, which doubles both width and height dimensions, ensuring the maintenance of a binary feature map. These are subsequently concatenated with feature maps (of congruent spatial dimensions) originating from the backbone. Within the network's holistic architecture, the feature pyramid module enhances the features, synergizing the backbone components, thereby fostering superior adaptability for intricate tasks at hand. These enhanced features navigate through a 1×1 convolution, followed by batch normalization and a spike activation function, thereby constituting the succeeding level of the feature pyramid. Spiking feature pyramid then interfaces with a multi-head prediction module through convolutional layers, batch normalization, and spike activation. The resultant features undergo a 1×1 convolution, yielding floating-point outcomes with a shape of $N \times N \times [3 \times (C + 5)]$, wherein N symbolizes the width and height of the pertinent feature map, C represents the number of classes, and the number 5 corresponds to four bounding box coordinate predictions complemented by a singular confidence prediction. The method of non-maximum suppression (NMS) [85], [86] is employed to finalize the bounding boxes.

2) *Neural Behavior and Adaptation*: In the realm of SNNs, the choice of the basic unit emerges as a pivotal aspect in network design. In fast-paced, event-based contexts, the adaptability to the conveyed information is our core concern. As such, we adopted an adaptively tunable spiking neuron model. To amplify its capacity to encapsulate information, we

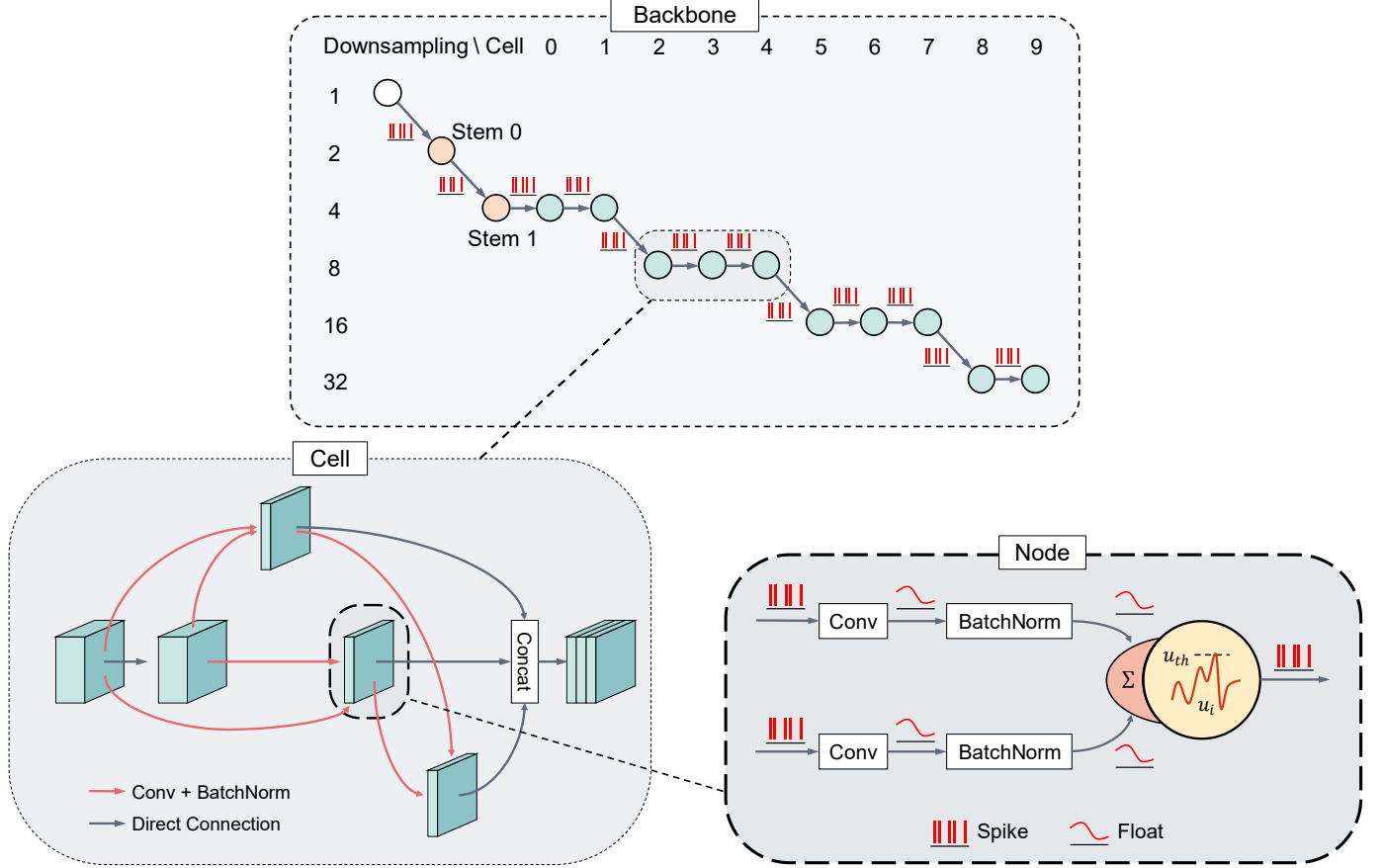


Fig. 2. Overview of the proposed encoder backbone. The structure adopts a multi-stage downsampling paradigm, incorporating multiple cells interlinked via directed acyclic graphs. The vertical annotations on the left delineate the downsampling scale associated with each cell structure, while the numbers atop the left side correspond to the cell's subscript, aligning with the detailed architecture showcased in Table I. Two spiking convolution layers, termed as stem layers, facilitate initial channel variations. The unique cell connection topology recurs across different layers. Operations within each cell, executed at the node level, accumulate on the membrane potential tier, culminating in a spiking generation function.

incorporated the iterative Leaky Integrate and Fire (LIF) model [15] as the foundational unit. This unit was then augmented with an agile threshold-adaptive mechanism, enhancing its representational capabilities for event data, as discussed below.

Leveraging its inherent temporal dynamics and sparse activation, the LIF neuron model's propagation pattern can be articulated as:

$$u_i^{(t,n)} = \tau \cdot u_i^{(t-1,n)} \cdot (1 - y_i^{(t-1,n)}) + I_i^{(t,n)}, \quad (2a)$$

$$I_i^{(t,n)} = \sum_j w_{ji} \cdot y_j^{(t,n-1)}, \quad (2b)$$

with the spike generation process is formulated with:

$$y_i^{(t,n)} = H(u_i^{(t,n)} - U_{th}) = \begin{cases} 1, & \text{if } u_i^{(t,n)} \geq U_{th} \\ 0, & \text{otherwise.} \end{cases} \quad (3)$$

where the $u_i^{(t,n)}$ represents the membrane potential of the neuron i of the n -th layer at time t , τ is a constant which represents the membrane time attenuation factor consequently configures the membrane leakage of the neuron, $I_i^{(t,n)}$ is the influx currency, which is essentially the weighted sum of the spiking activation $y_j^{(t,n-1)}$ generated from the connected

neurons from the previous layer $n - 1$. The spiking activation $y_i^{(t,n)}$ is defined by a Heaviside function $H(\cdot)$ which is calculated to be 1 only when $u_i^{(t,n)}$ reaches a membrane threshold U_{th} , otherwise remains 0.

Drawing inspiration from the adaptive behaviors of neurons in the neocortex [87], [88], our design incorporates the self-adaptive mechanism into the LIF spiking neuron. This adaptive threshold mechanism, which has been previously utilized in recurrent SNNs for temporal sequence learning [89], [90], introduces the capacity for longer memory retention. Notably, this mechanism has proven its adaptability in several experimental settings. Specifically, the adaptive threshold mechanism's propagation pattern can be described as:

$$y^{(t)} = H(u^{(t)} - A_{th}^{(t)}), \quad (4a)$$

$$A_{th}^{(t)} = U_{th} + \beta \cdot a^{(t)}, \quad (4b)$$

$$a^{(t)} = \tau_a \cdot a^{(t-1)} + y^{(t-1)}, \quad (4c)$$

where $H(\cdot)$ is the Heaviside step function. $A_{th}^{(t)}$ signifies the modifiable threshold at time t . Meanwhile, $a^{(t)}$ represents the evolving threshold increment, which is modulated by the neuron's spiking history. Here, β is a scaling coefficient, and τ_a is the time constant for a .

Crucially, the adjustable threshold A_{th} dynamically influences the spiking rate. When faced with intensive input, this threshold rises, thereby inhibiting the neuron's firing propensity. On the other hand, sparse input leads to a decrease in this threshold, making the neuron more prone to firing. By examining the limits of this adaptive mechanism under various input scenarios, we can discern its bounds. Under conditions where the neuron remains consistently inactive, as t approaches infinity, $a^{(t)}$ converges to 0. This implies that the lowest bound for $A_{\text{th}}^{(t)}$ is the base threshold U_{th} . However, in a contrasting scenario where the neuron is incessantly active (with initial conditions $y^{(0)} = 1$ and $a^{(0)} = 0$), the evolution of $a^{(t)}$ can be portrayed as:

$$a^{(t)} = \sum_{i=1}^t \tau_a^{(i-1)}, \quad (5)$$

and its upper limit, as t grows indefinitely, is determined to be $1/(1 - \tau_a)$. Hence, the adaptive threshold A_{th} spans from U_{th} to $U_{\text{th}} + \beta/(1 - \tau_a)$. This event-driven adaptivity augments the network's resilience and stability, especially in the face of swift alterations in event density.

C. Network Training

To capitalize on the temporal dynamics of spiking neurons, the initial obstacle is the intricacy of training SNNs. This challenge stems from the discontinuous nature of spike generation, such that the absence of a gradient renders backpropagation unfeasible.

Early strides in the application of deep SNNs to machine learning tasks were made by transferring parameters from ANN-trained models to corresponding SNNs [33], [34]. However, this method is confined to feed-forward architectures devoid of recurrency, making it suitable only for tasks with limited temporal dependencies. To overcome this limitation, we embrace surrogate gradient training. This method approximates the discontinuous activation by smoothening the spike generation function, as denoted in Eq. (3). This approximation permits gradient computation for backpropagation. During this training phase, temporal neural dynamics, as detailed in Eq. (2), are meticulously modeled, and the resulting errors are backpropagated through time. Consequently, surrogate gradient approximations not only facilitate the training of spiking neurons while considering their temporal intricacies but are also inherently apt for tasks with pronounced temporal dependencies, like the continuous object detection challenge we address. As a stand-in for the gradient of the spiking function, we utilize the Dispik function [18], given by:

$$\text{Dspike}(u) = a \cdot \tanh(b \cdot (u - c)) + d, \quad 0 \leq u \leq 1, \quad (6a)$$

$$\tanh(x) = \frac{e^x - e^{-x}}{e^x + e^{-x}}, \quad (6b)$$

where u denotes the membrane potential. The parameters (a, b, c, d) modify the intrinsic hyperbolic tangent function, \tanh , ensuring its output remains bounded within $[0, 1]$, while varying in shape. With a plethora of surrogate functions at our

disposal, catering to diverse training needs becomes feasible. The parameter b , termed the temperature factor, regulates the function's smoothness. Typically, c is fixed at 0.5, ensuring symmetrical behavior around $u = 0.5$. For our chosen variant of the Dispik function, it is ensured that both c and d are adjusted such that $\text{Dspike}(0) = 0$ and $\text{Dspike}(1) = 1$.

IV. EXPERIMENTS

This section delves into a comprehensive examination of our proposed SpikeFPN, underscoring its advantages through rigorous experimentation. Initially, we detail the training regimen of SpikeFPN on the GEN1 Automotive Detection (GAD) dataset [48], encompassing facets such as data preparation, hyper-parameter optimization, and comparative performance analysis. Subsequently, ablation studies elucidate the design decisions underpinning our model—highlighting the nuances of event data preprocessing and architectural considerations. Finally, capitalizing on the inherent sparse propagation properties of SNNs, we present a comparative analysis of SpikeFPN's computational efficiency and energy consumption.

A. Experiment on GAD

A comprehensive procedure encompassing data preparation, training, and testing has been executed on the GAD dataset, yielding noteworthy results. This section delineates the entire experimental procedure, beginning with the details of the input dataset and its encoding settings. This is followed by a discussion on the requisite hyper-parameters and performance evaluation metrics used during the training and testing phases, culminating in an evaluation of the outcomes.

1) *Input Data Representation*: The GAD dataset, obtained using a Prophesee GEN1 ATIS sensor, is an expansive event-based automotive object detection collection. It consists of over 39 hours of automotive recordings (with a resolution of 304×240). Alongside approximately 255,000 manually labeled bounding boxes at 1 Hz, 2 Hz, and 4 Hz denoting cars and pedestrians, the data is divided into training, validation, and test sets. The recordings are segmented into 60-second intervals, with each set containing 1460, 429, and 470 videos, respectively. During this experiment's training and testing phases, the data partitioning in GAD was meticulously followed to ensure accurate representation of results.

In real-world settings, the event data from the sensor is sequential and varies in length. For a more efficient implementation, we processed the variable-length event data through fixed-length segmentation. After encoding the event data, $S \times C$ frames preceding the label were created to be fed into the network for each sample in the following training. Here, S represents the number of stacks from the SBT framing process, and C is the number of frames in each stack. This frame-compression approach corresponds to what is presented in Eq. (1). With $\Delta t = 60$ ms, $n = C = 3$, and $S = 3$, the segmented event data is transformed into tensor-form data frames, preserving the time information between frames. The minimum temporal resolution here is $T = \Delta t/n = 20$ ms.

TABLE II
COMPARISON OF THE TWO MEAN AVERAGE PRECISION METRICS AND THE NETWORK PARAMETER QUANTITIES FOR DIFFERENT TYPES OF NETWORKS ON THE GEN1 AUTOMOTIVE DETECTION DATASET

Model	Network Type	Params (M)	timestep	mAP ₅₀	mAP _{50:95}
SparseConv [47]	ANN	133	-	0.149	-
Events-RetinaNet [9]	ANN	33	-	0.340	-
E2Vid-RetinaNet [9]	ANN	44	-	0.270	-
RED [9]	ANN	24	-	0.400	-
Gray-RetinaNet [9]	ANN	33	-	0.440	-
ASTMNet [10]	ANN	-	-	0.467	-
VGG-11 + SSD [20]	SNN	13	5	0.37*	0.174
MobileNet-64 + SSD [20]	SNN	24	5	0.35*	0.147
DenseNet121-24 + SSD [20]	SNN	8	5	0.38*	0.189
SpikeFPN (ours)	SNN	22	3	0.477	0.223

* Provided by the authors.

2) *Hyper-Parameters Setting*: For the training phase, we employed the AdamW optimizer with an initial learning rate of 0.001 and a weight decay of 0.0005. Pre-training was deemed unnecessary; hence, all models underwent direct training for 30 epochs with a batch size of 32. A warm-up policy was applied using the first epoch's learning rate, which initially starts at a nominal value and then gradually ascends to the prescribed learning rate. The LIF and ALIF neurons have a membrane time constant τ of 0.2 and a membrane threshold U_{th} of 0.3. The temperature b of the Dspike function is set at 3. For the ALIF neuron, β is 0.07, while τ_a is a learnable parameter constrained to [0.2, 0.4], initialized at 0.3. To assess the network's training error and gauge the model's performance, we opted for the mAP, setting the prediction score to 0.3 as the accuracy metric. For a more comprehensive evaluation, we employed two mAP-based metrics: mAP₅₀ and mAP_{50:95}. The former, mAP₅₀, represents the widely-accepted mean Average Precision with an overlap threshold of 0.5 [60], [91]. In contrast, mAP_{50:95} serves as an alternative metric, indicating the mean Average Precision across 10 IoU ranges ([.50:.05:.95]).

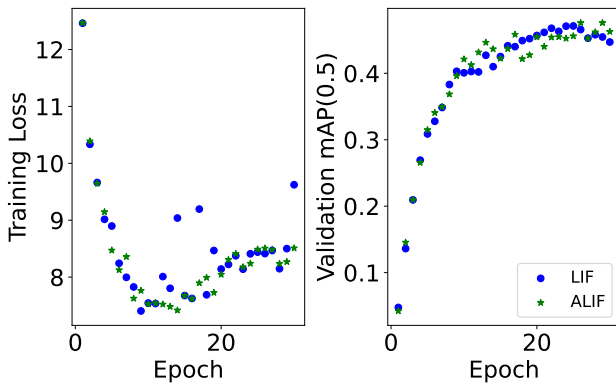


Fig. 3. Comparisons of training losses and validation mAPs of SNNs using LIF and ALIF neurons for the first layer.

3) *Results*: Throughout the training phase, the final stack output from the model serves as the prediction result. This approach ensures the preservation and accumulation of temporal information, crucial for the model's learning process and subsequent calculation of evaluation metrics. For clarity, we juxtaposed our methods against various SNN and ANN

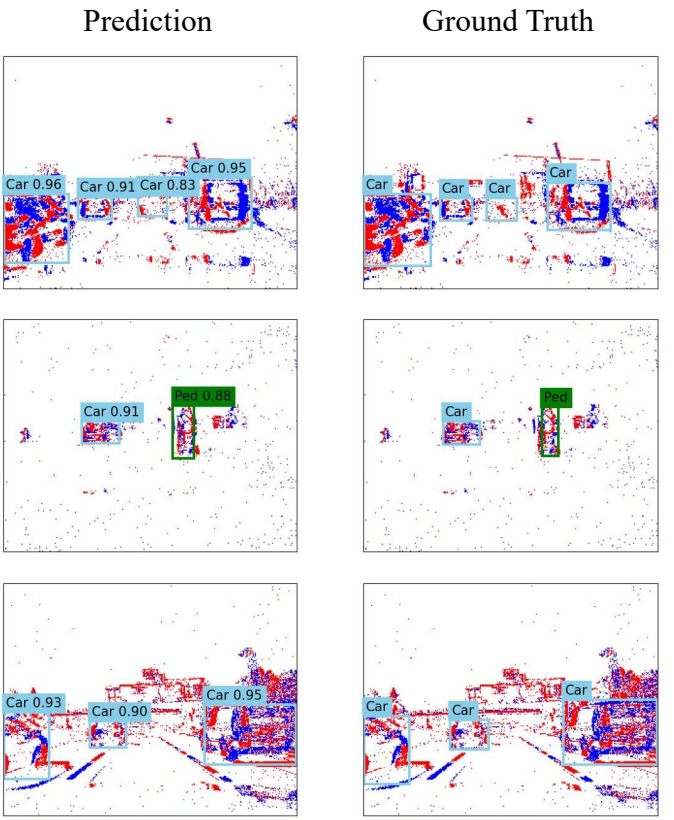


Fig. 4. The prediction results of SpikeFPN (left column) and the corresponding ground truth (right column). The "Ped" in each cell stands for the category of pedestrian.

models tested on the GAD dataset. These comparative results are tabulated in Table II, with values for other models sourced from existing literature.

From a SNN perspective, our proposed SpikeFPN markedly outperforms three preceding models discussed in [20]. It exhibits an improvement ranging from 9.7% to 12.7% for mAP₅₀ and between 3.4% to 7.6% for mAP_{50:95}. Remarkably, this is achieved with fewer requisite steps to convergence. An examination of the training loss between SNNs, especially when comparing LIF and ALIF neurons in the first layer (depicted in Fig. 3), reveals that the ALIF neuron fosters a more stable training trajectory than its LIF counterpart.

Moreover, our SpikeFPN's streamlined architecture modestly outpaces the ASTMNet [10], a state-of-the-art ANN incorporating attention mechanisms and bespoke adaptive sampling event preprocessing schemes.

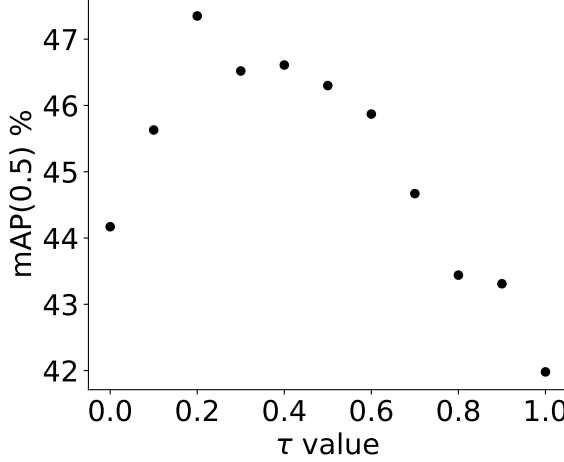


Fig. 5. A graph detailing the mean precision for LIF neurons at varying τ values. The results, averaged across three distinct experiments with varied random seeds, emphasize the influence of the membrane time constant on performance.

To assess our model's real-time capabilities, we continuously input the entire test split into the network. This process mirrors the length of steps, generating sequential labels. The average inference velocity for a single stack stands at 54 frames per second when operating on a Tesla V100 GPU. Such outcomes underscore both the efficacy of the SpikeFPN and the broader promise of SNNs in handling dynamic events coupled with sparse propagation. For further illustration, a selection of our model's prediction results can be perused in Fig. 4.

B. Ablation Study

In this subsection, we conduct ablation experiments from two aspects: the event coding paired with a basic neuron computation scheme, and the structure of the network itself. Through these, we aim to highlight the enhancements the proposed SpikeFPN brings to the table.

1) *Event Input Configuration*: Our goal here is to gauge the influence of varying preprocessing methods and input configurations on model performance. To this end, we juxtapose results obtained using SBE and SBT, both with LIF neurons. For each method, two input configurations, which are defined by different numbers of stacks (S) and frames within each stack (C), are employed: $S = 3, C = 3$ and $S = 2, C = 5$. With the SBT method, events within 20 ms are housed in each frame, while the SBE method's frame encapsulates 5000 events. Additionally, we introduce the Adaptive-LIF (ALIF) neuron to the initial layer in the SBT process, facilitating a comparison of neuron types across various input configurations. The findings are tabulated in Table III.

Preliminary observations indicate that the LIF neuron, when coupled with the SBE process, does not fare as well in terms of

accuracy compared to its performance with the SBT process. Interestingly, the configurations $S = 3, C = 3$ underperform relative to $S = 2, C = 5$ for both SBE and SBT. However, when SBT is paired with the ALIF neuron, the performance is optimized at $S = 3, C = 3$. In essence, the SBT process outperforms SBE in our model setup, and the ALIF neuron, when presented with a larger stack number, better modulates its threshold in the SBT process.

TABLE III
RESULTS WITH DIFFERENT INPUT CONFIGURATIONS. S AND C REPRESENT THE NUMBER OF STACKS AND THE NUMBER OF FRAMES IN EACH STACK RESPECTIVELY.

Method	S	C	mAP_{50}	$mAP_{50:95}$
SBE + LIF	2	5	0.4356	0.1970
SBE + LIF	3	3	0.4324	0.1944
SBT + LIF	2	5	0.4758	0.2224
SBT + LIF	3	3	0.4710	0.2176
SBT + ALIF	2	5	0.4731	0.2191
SBT + ALIF	3	3	0.4770	22.27

2) *ALIF Performance*: We further delve into the sensitivity of the adaptive threshold in ALIF concerning hyper-parameters and the merits of training τ_a . Our findings, summarized in Table IV, unequivocally show the robustness of performance across a spectrum of β values. Additionally, networks furnished with a trainable τ_a consistently outshine those with fixed counterparts.

TABLE IV
RESULTS WITH DIFFERENT HYPERPARAMETER SETTING OF THE ADAPTIVE THRESHOLD.

β	Initial τ_a	State of τ_a	mAP_{50}	$mAP_{50:95}$
0.07	0.3	non-trainable	0.470	0.219
0.09	0.3	trainable	0.471	0.220
0.05	0.3	trainable	0.473	0.217
0.07	0.3	trainable	0.477	0.223

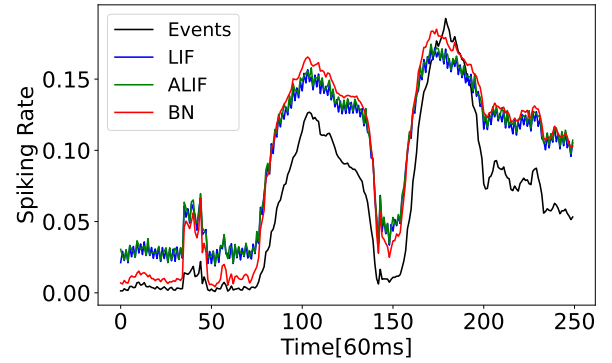


Fig. 6. Illustration of a sample sequence depicting event density alongside the first layer's activation for LIF $\tau = 0.2$, ALIF $\tau = 0.2$, and binary neurons (denoted as "BN" in the legend). Each point on the "Events" curve represents the average event density of an SBT stack over a duration of 60 ms. The layer activation is derived by averaging the resulting spiking feature map.

According to Eq. (2), the membrane time constant, τ , dictates the proportion of the prior timestep's membrane potential to retain. This attenuated accumulation addresses the sparse propagation issue. Fig. 6 depicts a sequence of input event

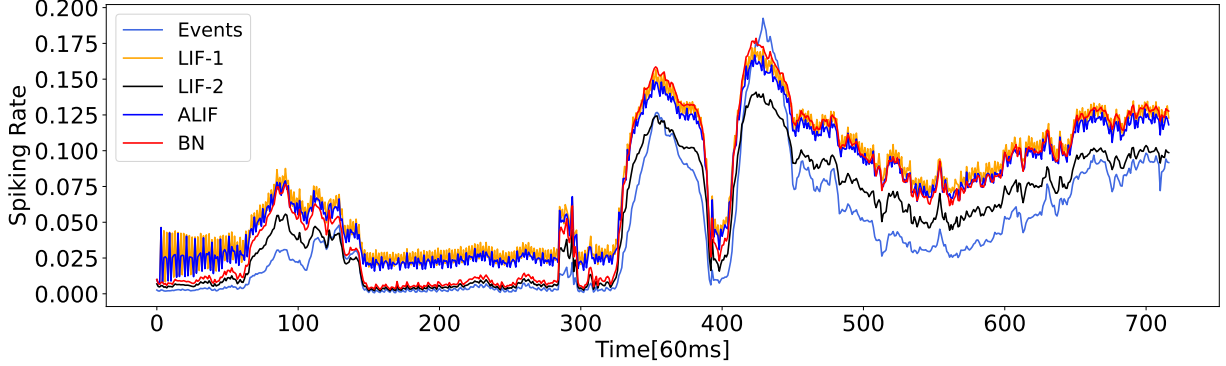


Fig. 7. Comparison of event density and layer activation across LIF, ALIF, and binary neurons. LIF-1 and LIF-2 denote LIF neurons with threshold values set to 0.3 and 0.4, respectively. Each data point on the “Events” curve represents the mean event density of an SBT stack spanning 60ms. Layer activation is determined by averaging the spiking feature map.

density compared to the first layer activation with different τ values. Layers with LIF neurons function akin to low-pass filters, especially when event density experiences sharp variations. In contrast, layers with binary neurons (where $\tau = 0$) tend to mirror their input closely, displaying synchronous changes. An exploration into the effect of the membrane time constant was undertaken, testing τ values from 0 to 1 at 0.1 intervals. With a set random seed for LIF neurons, mAP₅₀ values at τ of 0, 0.1, 0.2, and 0.3 were 0.4252, 0.4455, 0.4710, and 0.4696, respectively. This emphasizes the membrane potential constant’s impact on overall accuracy. Retaining prior timestep data, attenuated during temporal accumulation, proves beneficial. To corroborate the findings, additional experiments with three random seeds were executed for varying τ values. The resultant mAP₅₀ values were averaged and presented in Fig. 5, underscoring the advantages of self-adaptive thresholds during event encoding.

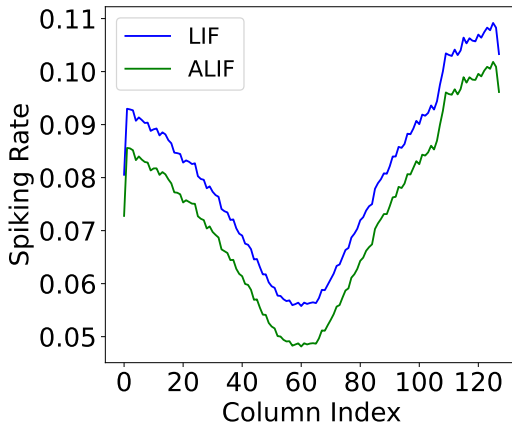


Fig. 8. Averaged column firing rate of the first layer on the GAD test set for LIF and ALIF neurons. Data was pooled from four experiments, each initiated with a different random seed. The mean mAP₅₀ values for LIF and ALIF neurons stand at 0.4662 ± 0.0029 and 0.4738 ± 0.0034 , respectively. The V-shaped pattern reflects fewer events from distant objects, particularly at the valley.

When using different random seeds, the network with the first layer utilizing ALIF neurons consistently surpassed net-

works with LIF neurons at 0.3 and 0.4 thresholds, as detailed in Section IV-A. This accentuates the adaptive threshold’s capability in managing dynamic events. In the context of firing rate, the ALIF neuron leads to increased layer sparsity, as seen in Fig. 8, emphasizing the merits of self-adjusting thresholds in event encoding.

TABLE V
RESULTS ON THE GAD DATASET WHEN APPLYING DIFFERENT NEURON MODEL ON THE FIRST AND ALL LAYERS OF THE NETWORK.

Neuron	Layer	Threshold	mAP ₅₀
LIF	All/First	0.3	0.470 ± 0.001
	First	0.4	0.470
ALIF	All	0.3	0.400
	First	0.3	0.476 ± 0.002

In pursuit of optimal neuron placement for the adjustable threshold, we compared the performance of models employing LIF and adaptive threshold LIF (ALIF) neurons. Experiments were conducted using ALIF neurons across the entire network and exclusively on the first layer, with subsequent layers using LIF neurons. During these trials, we treated τ_a as a trainable variable, consistent across layers. Outcomes are summarized in Table V. However, integrating ALIF neurons throughout the network led to subpar outcomes. Over-reliance on adjustable thresholds might infuse excessive flexibility, thereby hampering training precision. For clarity, Fig. 7 presents an input event stream sequence by event density, juxtaposed with the first layer’s activation using distinct neuron models. The LIF layer with $U_{th} = 0.4$ exhibits the least activation, whereas the binary neuron layer with $U_{th} = 0.3$ shows significant fluctuations. In comparison, both LIF and ALIF layers provide a moderating effect over input variations. The ALIF layer’s activation resides between the LIF layers’ threshold bounds, attributed to the adaptive threshold properties, emphasizing ALIF’s potential in enhancing both layer sparsity and accuracy.

3) *Spiking ResNet*: In this ablation study segment, we designed a spike-based ResNet-18 encoder backbone. Distinctive features include variable initial channel sizes, incorporation of the feature pyramid, a multi-head prediction module, and substitution of all activation functions with the Heaviside function $H(\cdot)$, referenced in Eq. (3). This network, adhering

TABLE VI

RESULTS ON GAD DATASET WITH DIFFERENT BACKBONE ARCHITECTURES. THE ACRONYM “ICS” STANDS FOR THE INITIAL CHANNEL SIZE.

Architecture	ICS	Model size (M)	mAP ₅₀	mAP _{50:95}
ResNet18	64	13.34	0.4163	0.1799
ResNet18	80	20.82	0.4208	0.1896
ResNet18	96	29.97	0.4429	0.1992
SpikeFPN (ours)	48	21.63	0.4770	0.2227

to a 4-stage downsampling blueprint, adopts its residual block from [19], [92]. Outputs from the last blocks of stages 2, 3, and 4 are relayed to the feature pyramid. The network’s maximum downsampling ratio stands at 32. The architecture specifics, when initiated with 80 channels, are tabulated in Table VII. Assessing our encoder’s design efficacy, we paralleled it with this variant, given its analogous downsampling approach. Different channel sizes were evaluated to represent diverse model capacities, with findings consolidated in Table VI. Remarkably, when juxtaposed under similar model parameters, ResNet (initialized with 80 channels) marginally underperforms against SpikeFPN. A plausible explanation could be SpikeFPN’s extensive intra and inter-cell connections, fostering gradient and information flow throughout the SNN training.

TABLE VII

DETAILED ARCHITECTURE OF THE MANUALLY CONSTRUCTED SPIKE-BASED RESNET, INCLUDING THE ENCODER BACKBONE OF RESNET-18, THE FEATURE PYRAMID AND THE MULTI-HEAD PREDICTION MODULE. C DENOTES THE NUMBER OF CLASSES AND K DENOTES THE NUMBER OF ANCHORS.

Module	Layer	Output Feature Map $c \times h \times w$
Backbone	Stem 0	$80 \times 128 \times 128$
	Stem 1	$80 \times 64 \times 64$
	Layer 1-1	$80 \times 64 \times 64$
	Layer 1-2	$80 \times 64 \times 64$
	Layer 2-1	$160 \times 32 \times 32$
	Layer 2-2	$160 \times 32 \times 32$
	Layer 3-1	$320 \times 16 \times 16$
	Layer 3-2	$320 \times 16 \times 16$
	Layer 4-1	$640 \times 8 \times 8$
	Layer 4-2	$640 \times 8 \times 8$
Feature Pyramid	Layer 2-2 → p1	$80 \times 32 \times 32$
	Layer 3-2 → p2	$160 \times 16 \times 16$
	Layer 4-2 → p3	$320 \times 8 \times 8$
Multi-Head Prediction	p1 → d1	$K \times (C + 5) \times 32 \times 32$
	p2 → d2	$K \times (C + 5) \times 16 \times 16$
	p3 → d3	$K \times (C + 5) \times 8 \times 8$

C. Network Sparsity and Computation Cost

SNNs inherently harness the potential of spike-based sparse computations and eschew multiplicative inferences, ensuring a pronounced computational edge over their ANN counterparts, which are predicated on dense matrix multiplication. To elucidate this, we compared the SpikeFPN’s computational efficiency against existing ANN and SNN benchmarks.

As illustrated in Fig. 9, SpikeFPN is characterized by varied sparsity across layers. Comprehensive sparsity metrics and computational costs are detailed in Table VIII. Evidently, our SpikeFPN outshines contemporaneous spiking neural networks

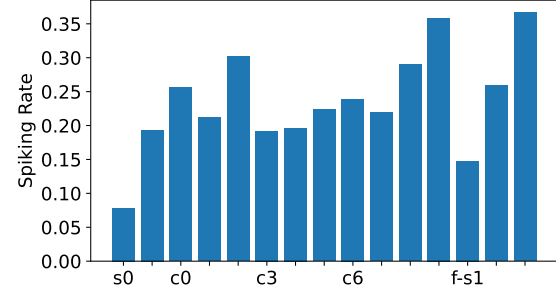


Fig. 9. The spiking sparsity of SpikeFPN. The network exhibits an overall sparse activity with varying degrees across layers, with the highest sparsity at the first layer due to highly sparse input event streams.

in automotive object detection tasks, achieving greater sparsity and fewer operations.

TABLE VIII

COMPARISON OF OPERATION NUMBER (OP) AND ESTIMATED ENERGY COST. FOR SNN NUMBER OF ADDITION OPERATIONS IS COUNTED AND FOR ANN NUMBER OF MULTIPLICATION-ADDITION OPERATIONS IS COUNTED.

Model	# OP.	Sparsity	Energy (mJ)
Events-RetinaNet (ANN)	18.73G	-	86.16
VGG-11 + SDD	12.30G	22.22%	11.07
MobileNet-64 + SSD	6.39G	29.44%	5.74
DenseNet121-24 + SSD	4.33G	37.20%	3.90
SpikeFPN (ours)	2.83G	19.10%	2.55

Adopting methodologies from [16], [18], [93], SNN addition operations are quantified using $s \times T \times A$, where s signifies mean sparsity, T represents timestep, and A accounts for additions per iteration. Energy estimations are predicated on [94]’s examination of 45 nm CMOS technology, as adopted in works like [16], [18], [64]. Here, SNN addition operations cost 0.9 pJ, whereas ANN MAC operations demand 4.6 pJ. We benchmarked against Events-RetinaNet [9] given its accessible codebase, facilitating a balanced comparison. Notably, compared to Events-RetinaNet, SpikeFPN demonstrates a nearly 6-fold reduction in operations and a 33-fold decrease in energy consumption. Such frugality underscores the SNN’s potential in energy-efficient, event-driven vision tasks.

V. CONCLUSIONS

The presented research introduces the SpikeFPN, a novel architecture that seamlessly combines a spiking feature pyramid network with a self-adaptive spiking neuron. This design specifically targets event-based automotive object detection tasks by harnessing the unique capability of the self-adaptive spiking neurons to encode sparse data effectively. The adoption of such architecture, an area of burgeoning interest, has delivered impressive outcomes in terms of both detection accuracy and computational efficiency.

Extensive experimentation using the GEN1 Automotive Detection dataset underscores the efficiency and validity of our proposed model. These experimental results depict not only a commendable mAP prediction accuracy, but also the sound reasoning behind the SpikeFPN’s design. In drawing

comparisons with similar network structures, inclusive of non-adaptive and various downsampling configurations, our SpikeFPN demonstrates consistent robustness across varying problem sizes. Theoretical insights further reveal the benefits of the spiking mechanism-based model, particularly highlighting its low power consumption and reduced computational demands, suggesting its potential utility for applications demanding efficient computational paradigms.

In summation, the integration of self-adaptive spiking mechanisms within the feature pyramid network structure presents a promising avenue for advancing event-based visual tasks. Given the inherent discrete and sparse nature of events, and the added advantage of preserving temporal information, aligning this data format with our unique neuron setup might pave the way for notable performance enhancements. The inherent low power consumption attributed to the sparse propagation properties of spiking neurons, when combined with our experimental outcomes, suggests a possible edge that SNNs could hold over traditional architectures in specific domains. Such potential merits further exploration and research.

REFERENCES

- [1] L. Liu, W. Ouyang, X. Wang, P. Fieguth, J. Chen, X. Liu, and M. Pietikäinen, “Deep learning for generic object detection: A survey,” *International Journal of Computer Vision*, vol. 128, no. 2, pp. 261–318, Feb. 2020.
- [2] Z. Zou, K. Chen, Z. Shi, Y. Guo, and J. Ye, “Object detection in 20 years: A survey,” 2023.
- [3] P. Lichtsteiner, C. Posch, and T. Delbrück, “A 128×128 120 db $15\mu s$ latency asynchronous temporal contrast vision sensor,” *IEEE journal of solid-state circuits*, vol. 43, no. 2, pp. 566–576, 2008.
- [4] C. Posch, D. Matolin, and R. Wohlgemant, “A qvga 143 db dynamic range frame-free pwm image sensor with lossless pixel-level video compression and time-domain cds,” *IEEE Journal of Solid-State Circuits*, vol. 46, no. 1, pp. 259–275, 2010.
- [5] S. Chen, W. Tang, X. Zhang, and E. Culurciello, “A 64×64 pixels uwb wireless temporal-difference digital image sensor,” *IEEE transactions on very large scale integration (VLSI) systems*, vol. 20, no. 12, pp. 2232–2240, 2011.
- [6] T. Serrano-Gotarredona and B. Linares-Barranco, “A 128×128 1.5% contrast sensitivity 0.9% fpn $3 \mu s$ latency 4 mw asynchronous frame-free dynamic vision sensor using transimpedance preamplifiers,” *IEEE Journal of Solid-State Circuits*, vol. 48, no. 3, pp. 827–838, 2013.
- [7] C. Brandli, R. Berner, M. Yang, S.-C. Liu, and T. Delbrück, “A 240×180 130 db $3 \mu s$ latency global shutter spatiotemporal vision sensor,” *IEEE Journal of Solid-State Circuits*, vol. 49, no. 10, pp. 2333–2341, 2014.
- [8] B. Son, Y. Suh, S. Kim, H. Jung, J. S. Kim, C. Shin, K. Park, K. Lee, J. Park, J. Woo *et al.*, “4.1 a 640×480 dynamic vision sensor with a $9\mu m$ pixel and 300meps address-event representation,” in *2017 IEEE International Solid-State Circuits Conference (ISSCC)*. IEEE, 2017, pp. 66–67.
- [9] E. Perot, P. de Tournemire, D. Nitti, J. Masci, and A. Sironi, “Learning to detect objects with a 1 megapixel event camera,” *Advances in Neural Information Processing Systems*, vol. 33, pp. 16 639–16 652, 2020.
- [10] J. Li, J. Li, L. Zhu, X. Xiang, T. Huang, and Y. Tian, “Asynchronous spatio-temporal memory network for continuous event-based object detection,” *IEEE Transactions on Image Processing*, vol. 31, pp. 2975–2987, 2022.
- [11] S. GHOSH-DASTIDAR and H. ADELI, “Spiking neural networks,” *International Journal of Neural Systems*, vol. 19, no. 04, pp. 295–308, 2009, pMID: 19731402. [Online]. Available: <https://doi.org/10.1142/S0129065709002002>
- [12] K. Roy, A. Jaiswal, and P. Panda, “Towards spike-based machine intelligence with neuromorphic computing,” *Nature*, vol. 575, no. 7784, pp. 607–617, Nov. 2019.
- [13] F. Zenke and S. Ganguli, “Superspike: Supervised learning in multilayer spiking neural networks,” *Neural computation*, vol. 30, no. 6, pp. 1514–1541, 2018.
- [14] E. O. Neftci, H. Mostafa, and F. Zenke, “Surrogate gradient learning in spiking neural networks: Bringing the power of gradient-based optimization to spiking neural networks,” *IEEE Signal Processing Magazine*, vol. 36, no. 6, pp. 51–63, 2019.
- [15] Y. Wu, L. Deng, G. Li, J. Zhu, Y. Xie, and L. Shi, “Direct training for spiking neural networks: Faster, larger, better,” in *Proceedings of the AAAI Conference on Artificial Intelligence*, vol. 33, no. 01, 2019, pp. 1311–1318.
- [16] N. Rathi and K. Roy, “Diet-snn: A low-latency spiking neural network with direct input encoding and leakage and threshold optimization,” *IEEE Transactions on Neural Networks and Learning Systems*, 2021.
- [17] H. Zheng, Y. Wu, L. Deng, Y. Hu, and G. Li, “Going deeper with directly-trained larger spiking neural networks,” in *Proceedings of the AAAI Conference on Artificial Intelligence*, vol. 35, no. 12, 2021, pp. 11 062–11 070.
- [18] Y. Li, Y. Guo, S. Zhang, S. Deng, Y. Hai, and S. Gu, “Differentiable spike: Rethinking gradient-descent for training spiking neural networks,” *Advances in Neural Information Processing Systems*, vol. 34, pp. 23 426–23 439, 2021.
- [19] S. Deng, Y. Li, S. Zhang, and S. Gu, “Temporal efficient training of spiking neural network via gradient re-weighting,” *arXiv preprint arXiv:2202.11946*, 2022.
- [20] L. Cordone, B. Miramond, and P. Thierion, “Object detection with spiking neural networks on automotive event data,” 2022.
- [21] R. Pérez, F. Schubert, R. Rasshofer, and E. Biebl, “Deep learning radar object detection and classification for urban automotive scenarios,” in *2019 Kleinheubach Conference*, 2019, pp. 1–4.
- [22] M. Ulrich, S. Braun, D. Köhler, D. Niederlöhrner, F. Faion, C. Gläser, and H. Blume, “Improved orientation estimation and detection with hybrid object detection networks for automotive radar,” in *2022 IEEE 25th International Conference on Intelligent Transportation Systems (ITSC)*, 2022, pp. 111–117.
- [23] C. Chen, J. Song, C. Peng, G. Wang, and Y. Fang, “A novel video salient object detection method via semisupervised motion quality perception,” *IEEE Transactions on Circuits and Systems for Video Technology*, vol. 32, no. 5, pp. 2732–2745, 2022.
- [24] G. Brazil and X. Liu, “M3d-rpn: Monocular 3d region proposal network for object detection,” in *Proceedings of the IEEE/CVF International Conference on Computer Vision (ICCV)*, October 2019.
- [25] Y. Gong, X. Yu, Y. Ding, X. Peng, J. Zhao, and Z. Han, “Effective fusion factor in fpn for tiny object detection,” in *Proceedings of the IEEE/CVF Winter Conference on Applications of Computer Vision (WACV)*, January 2021, pp. 1160–1168.
- [26] D. Liang, Q. Geng, Z. Wei, D. A. Vorontsov, E. L. Kim, M. Wei, and H. Zhou, “Anchor retouching via model interaction for robust object detection in aerial images,” *IEEE Transactions on Geoscience and Remote Sensing*, vol. 60, pp. 1–13, 2022.
- [27] C. Chen, J. Wei, C. Peng, and H. Qin, “Depth-quality-aware salient object detection,” *IEEE Transactions on Image Processing*, vol. 30, pp. 2350–2363, 2021.
- [28] J. Hagenaars, F. Paredes-Vallés, and G. De Croon, “Self-supervised learning of event-based optical flow with spiking neural networks,” *Advances in Neural Information Processing Systems*, vol. 34, 2021.
- [29] S. Kim, S. Park, B. Na, and S. Yoon, “Spiking-yolo: spiking neural network for energy-efficient object detection,” in *Proceedings of the AAAI Conference on Artificial Intelligence*, vol. 34, no. 07, 2020, pp. 11 270–11 277.
- [30] T. Bu, W. Fang, J. Ding, P. Dai, Z. Yu, and T. Huang, “Optimal ann-snn conversion for high-accuracy and ultra-low-latency spiking neural networks,” in *International Conference on Learning Representations*, 2021.
- [31] Y. Li, S. Deng, X. Dong, R. Gong, and S. Gu, “A free lunch from ann: Towards efficient, accurate spiking neural networks calibration,” in *International Conference on Machine Learning*. PMLR, 2021, pp. 6316–6325.
- [32] J. Ding, Z. Yu, Y. Tian, and T. Huang, “Optimal ann-snn conversion for fast and accurate inference in deep spiking neural networks,” 2021.
- [33] B. Rueckauer, I.-A. Lungu, Y. Hu, M. Pfeiffer, and S.-C. Liu, “Conversion of Continuous-Valued Deep Networks to Efficient Event-Driven Networks for Image Classification,” *Frontiers in Neuroscience*, vol. 11, p. 682, 2017.
- [34] P. U. Diehl, D. Neil, J. Binas, M. Cook, S.-C. Liu, and M. Pfeiffer, “Fast-classifying, high-accuracy spiking deep networks through weight and threshold balancing,” in *2015 International joint conference on neural networks (IJCNN)*. IEEE, 2015, pp. 1–8.
- [35] X. Lagorce, G. Orchard, F. Galluppi, B. E. Shi, and R. B. Benosman, “Hots: a hierarchy of event-based time-surfaces for pattern recognition,”

IEEE transactions on pattern analysis and machine intelligence, vol. 39, no. 7, pp. 1346–1359, 2016.

[36] A. I. Maqueda, A. Loquercio, G. Gallego, N. García, and D. Scaramuzza, “Event-based vision meets deep learning on steering prediction for self-driving cars,” in *Proceedings of the IEEE Conference on Computer Vision and Pattern Recognition*, 2018, pp. 5419–5427.

[37] D. P. Moeyns, F. Corradi, E. Kerr, P. Vance, G. Das, D. Neil, D. Kerr, and T. Delbrück, “Steering a predator robot using a mixed frame/event-driven convolutional neural network,” in *2016 Second International Conference on Event-based Control, Communication, and Signal Processing (EBCCSP)*. IEEE, 2016, pp. 1–8.

[38] C. Ye, A. Mitrokhin, C. Parameshwara, C. Fermüller, J. Yorke, and Y. Aloimonos, “Unsupervised learning of dense optical flow and depth from sparse event data. corr abs/1809.08625 (2018).” 1809.

[39] A. Z. Zhu, L. Yuan, K. Chaney, and K. Daniilidis, “Ev-flownet: Self-supervised optical flow estimation for event-based cameras,” *arXiv preprint arXiv:1802.06898*, 2018.

[40] A. Nguyen, T. T. Do, D. G. Caldwell, and N. G. Tsagarakis, “Real-time 6dof pose relocalization for event cameras with stacked spatial lstm networks,” in *Proceedings of the IEEE/CVF Conference on Computer Vision and Pattern Recognition Workshops*, 2019, pp. 0–0.

[41] L. Wang, Y.-S. Ho, K.-J. Yoon *et al.*, “Event-based high dynamic range image and very high frame rate video generation using conditional generative adversarial networks,” in *Proceedings of the IEEE/CVF Conference on Computer Vision and Pattern Recognition*, 2019, pp. 10 081–10 090.

[42] A. Z. Zhu, L. Yuan, K. Chaney, and K. Daniilidis, “Unsupervised event-based learning of optical flow, depth, and egomotion,” in *Proceedings of the IEEE/CVF Conference on Computer Vision and Pattern Recognition*, 2019, pp. 989–997.

[43] S. Tulyakov, F. Fleuret, M. Kiefel, P. Gehler, and M. Hirsch, “Learning an event sequence embedding for dense event-based deep stereo,” in *Proceedings of the IEEE/CVF International Conference on Computer Vision*, 2019, pp. 1527–1537.

[44] M. Cannici, M. Ciccone, A. Romanoni, and M. Matteucci, “A differentiable recurrent surface for asynchronous event-based data,” in *European Conference on Computer Vision*. Springer, 2020, pp. 136–152.

[45] K. Zhang, K. Che, J. Zhang, J. Cheng, Z. Zhang, Q. Guo, and L. Leng, “Discrete time convolution for fast event-based stereo,” in *Proceedings of the IEEE/CVF Conference on Computer Vision and Pattern Recognition*, 2022, pp. 8676–8686.

[46] C. Scheerlinck, N. Barnes, and R. Mahony, “Asynchronous spatial image convolutions for event cameras,” *IEEE Robotics and Automation Letters*, vol. 4, no. 2, pp. 816–822, 2019.

[47] N. Messikommer, D. Gehrig, A. Loquercio, and D. Scaramuzza, “Event-based asynchronous sparse convolutional networks,” in *European Conference on Computer Vision*. Springer, 2020, pp. 415–431.

[48] P. de Tournemire, D. Nitti, E. Perot, D. Migliore, and A. Sironi, “A large scale event-based detection dataset for automotive,” 2020.

[49] P. A. Merolla, J. V. Arthur, R. Alvarez-Icaza, A. S. Cassidy, J. Sawada, F. Akopyan, B. L. Jackson, N. Imam, C. Guo, Y. Nakamura *et al.*, “A million spiking-neuron integrated circuit with a scalable communication network and interface,” *Science*, vol. 345, no. 6197, pp. 668–673, 2014.

[50] S. B. Furber, F. Galluppi, S. Temple, and L. A. Plana, “The spinnaker project,” *Proceedings of the IEEE*, vol. 102, no. 5, pp. 652–665, 2014.

[51] L. Leng, “Deep learning architectures for neuromorphic hardware,” Ph.D. dissertation, Master thesis, Ruprecht-Karls-Universität Heidelberg, 2014. HD-KIP 14-26, 2014.

[52] L. Leng, M. A. Petrovici, R. Martel, I. Bytschok, O. Breitwieser, J. Bill, J. Schemmel, and K. Meier, “Spiking neural networks as superior generative and discriminative models,” *Cosyne Abstracts, Salt Lake City USA*, 2016.

[53] L. Leng, R. Martel, O. Breitwieser, I. Bytschok, W. Senn, J. Schemmel, K. Meier, and M. A. Petrovici, “Spiking neurons with short-term synaptic plasticity form superior generative networks,” *Scientific reports*, vol. 8, no. 1, pp. 1–11, 2018.

[54] A. F. Kungl, S. Schmitt, J. Klähn, P. Müller, A. Baumbach, D. Dold, A. Kugele, E. Müller, C. Koke, M. Kleider *et al.*, “Accelerated physical emulation of bayesian inference in spiking neural networks,” *Frontiers in neuroscience*, p. 1201, 2019.

[55] L. Leng, “Solving machine learning problems with biological principles,” Ph.D. dissertation, 2020.

[56] M. Davies, A. Wild, G. Orchard, Y. Sandamirskaya, G. A. F. Guerra, P. Joshi, P. Plank, and S. R. Risbud, “Advancing neuromorphic computing with loihi: A survey of results and outlook,” *Proceedings of the IEEE*, vol. 109, no. 5, pp. 911–934, 2021.

[57] K. Roy, A. Jaiswal, and P. Panda, “Towards spike-based machine intelligence with neuromorphic computing,” *Nature*, vol. 575, no. 7784, pp. 607–617, 2019.

[58] A. Sengupta, Y. Ye, R. Wang, C. Liu, and K. Roy, “Going deeper in spiking neural networks: Vgg and residual architectures,” *Frontiers in neuroscience*, vol. 13, p. 95, 2019.

[59] M. Everingham, L. Van Gool, C. K. Williams, J. Winn, and A. Zisserman, “The pascal visual object classes (voc) challenge,” *International journal of computer vision*, vol. 88, no. 2, pp. 303–338, 2010.

[60] T.-Y. Lin, M. Maire, S. Belongie, J. Hays, P. Perona, D. Ramanan, P. Dollár, and C. L. Zitnick, “Microsoft coco: Common objects in context,” in *European conference on computer vision*. Springer, 2014, pp. 740–755.

[61] S. B. Shrestha and G. Orchard, “Slayer: Spike layer error reassignment in time,” *Advances in neural information processing systems*, vol. 31, 2018.

[62] W. Zhang and P. Li, “Temporal spike sequence learning via backpropagation for deep spiking neural networks,” *Advances in Neural Information Processing Systems*, vol. 33, pp. 12 022–12 033, 2020.

[63] L. Zhu, X. Wang, Y. Chang, J. Li, T. Huang, and Y. Tian, “Event-based video reconstruction via potential-assisted spiking neural network,” *arXiv preprint arXiv:2201.10943*, 2022.

[64] K. Che, L. Leng, K. Zhang, J. Zhang, Q. Meng, J. Cheng, Q. Guo, and J. Liao, “Differentiable hierarchical and surrogate gradient search for spiking neural networks,” *Advances in Neural Information Processing Systems*, vol. 35, pp. 24 975–24 990, 2022.

[65] R. Zhang, L. Leng, K. Che, H. Zhang, J. Cheng, Q. Guo, J. Liao, and R. Cheng, “Accurate and efficient event-based semantic segmentation using adaptive spiking encoder-decoder network,” *arXiv preprint arXiv:2304.11857*, 2023.

[66] B. Li, L. Leng, R. Cheng, S. Shen, K. Zhang, J. Zhang, and J. Liao, “Efficient deep spiking multi-layer perceptrons with multiplication-free inference,” *arXiv preprint arXiv:2306.12465*, 2023.

[67] K. He, X. Zhang, S. Ren, and J. Sun, “Spatial pyramid pooling in deep convolutional networks for visual recognition,” *IEEE transactions on pattern analysis and machine intelligence*, vol. 37, no. 9, pp. 1904–1916, 2015.

[68] T.-Y. Lin, P. Dollar, R. Girshick, K. He, B. Hariharan, and S. Belongie, “Feature pyramid networks for object detection,” in *Proceedings of the IEEE Conference on Computer Vision and Pattern Recognition (CVPR)*, July 2017.

[69] Z. Q. Zhao, P. Zheng, S. T. Xu, and X. Wu, “Object detection with deep learning: A review,” *IEEE Transactions on Neural Networks and Learning Systems*, vol. 30, no. 11, pp. 3212–3232, 2019.

[70] T.-Y. Lin, P. Dollar, R. Girshick, K. He, B. Hariharan, and S. Belongie, “Feature pyramid networks for object detection,” in *Proceedings of the IEEE Conference on Computer Vision and Pattern Recognition (CVPR)*, July 2017.

[71] S. Huang, Z. Lu, R. Cheng, and C. He, “Fapn: Feature-aligned pyramid network for dense image prediction,” in *Proceedings of the IEEE/CVF International Conference on Computer Vision (ICCV)*, October 2021, pp. 864–873.

[72] W. Liu, D. Anguelov, D. Erhan, C. Szegedy, S. Reed, C.-Y. Fu, and A. C. Berg, “SSD: Single shot MultiBox detector,” in *Computer Vision – ECCV 2016*. Springer International Publishing, 2016, pp. 21–37. [Online]. Available: https://doi.org/10.1007%2F978-3-319-46448-0_2

[73] S. Ren, K. He, R. Girshick, and J. Sun, “Faster r-cnn: Towards real-time object detection with region proposal networks,” 2016.

[74] K. He, G. Gkioxari, P. Dollár, and R. Girshick, “Mask r-cnn,” 2018.

[75] Z. Cai and N. Vasconcelos, “Cascade r-cnn: Delving into high quality object detection,” 2017.

[76] T. Y. Lin, P. Goyal, R. Girshick, K. He, and P. Dollár, “Focal loss for dense object detection,” 2018.

[77] J. Redmon and A. Farhadi, “Yolov3: An incremental improvement,” 2018.

[78] S. Liu, L. Qi, H. Qin, J. Shi, and J. Jia, “Path aggregation network for instance segmentation,” 2018.

[79] S. Liu, D. Huang, and Y. Wang, “Learning spatial fusion for single-shot object detection,” 2019.

[80] G. Ghiasi, T. Y. Lin, R. Pang, and Q. V. Le, “Nas-fpn: Learning scalable feature pyramid architecture for object detection,” 2019.

[81] M. Tan, R. Pang, and Q. V. Le, “Efficientdet: Scalable and efficient object detection,” 2020.

[82] S. Qiao, L. C. Chen, and A. Yuille, “Detectors: Detecting objects with recursive feature pyramid and switchable atrous convolution,” 2020.

- [83] Q. Fu and H. Dong, "Spiking neural network based on multi-scale saliency fusion for breast cancer detection," *Entropy*, vol. 24, no. 11, 2022. [Online]. Available: <https://www.mdpi.com/1099-4300/24/11/1543>
- [84] S. Ioffe and C. Szegedy, "Batch normalization: Accelerating deep network training by reducing internal covariate shift," in *International Conference on Machine Learning*. PMLR, 2015, pp. 448–456.
- [85] J. Redmon and A. Farhadi, "Yolo9000: better, faster, stronger," in *Proceedings of the IEEE conference on computer vision and pattern recognition*, 2017, pp. 7263–7271.
- [86] R. Girshick, J. Donahue, T. Darrell, and J. Malik, "Rich feature hierarchies for accurate object detection and semantic segmentation," in *Proceedings of the IEEE conference on computer vision and pattern recognition*, 2014, pp. 580–587.
- [87] W. Gerstner, W. M. Kistler, R. Naud, and L. Paninski, *Neuronal dynamics: From single neurons to networks and models of cognition*. Cambridge University Press, 2014.
- [88] N. W. Gouwens, J. Berg, D. Feng, S. A. Sorensen, H. Zeng, M. J. Hawrylycz, C. Koch, and A. Arkhipov, "Systematic generation of biophysically detailed models for diverse cortical neuron types," *Nature communications*, vol. 9, no. 1, p. 710, 2018.
- [89] G. Bellec, D. Salaj, A. Subramoney, R. Legenstein, and W. Maass, "Long short-term memory and learning-to-learn in networks of spiking neurons," *Advances in neural information processing systems*, vol. 31, 2018.
- [90] G. Bellec, F. Scherr, A. Subramoney, E. Hajek, D. Salaj, R. Legenstein, and W. Maass, "A solution to the learning dilemma for recurrent networks of spiking neurons," *Nature communications*, vol. 11, no. 1, p. 3625, 2020.
- [91] M. Everingham, L. Van Gool, C. K. I. Williams, J. Winn, and A. Zisserman, "The pascal visual object classes (VOC) challenge," *International Journal of Computer Vision*, vol. 88, no. 2, pp. 303–338, Jun. 2010.
- [92] W. Fang, Z. Yu, Y. Chen, T. Huang, T. Masquelier, and Y. Tian, "Deep residual learning in spiking neural networks," *Advances in Neural Information Processing Systems*, vol. 34, 2021.
- [93] Y. Kim, J. Chough, and P. Panda, "Beyond classification: Directly training spiking neural networks for semantic segmentation," *arXiv preprint arXiv:2110.07742*, 2021.
- [94] M. Horowitz, "1.1 computing's energy problem (and what we can do about it)," in *2014 IEEE International Solid-State Circuits Conference - Digest of Technical Papers (ISSCC)*. IEEE, 2014, pp. 10–14.